Inhibition of SIRT1 signaling sensitizes the antitumor activity of silybin against human lung adenocarcinoma cells in vitro and in vivo

Zhenxing Liang[1*], Yang Yang[1*], Haibin Wang[2*], Wei Yi[1], Xiaolong Yan[3], Juanjuan Yan[4], Yue Li[1], Yingtong Feng[3], Shiqiang Yu[1], Jian Yang[1], Zhenxiao Jin[1], Weixun Duan[1#], and Wensheng Chen[1#]

[1]Department of Cardiovascular Surgery, Xijing Hospital, The Fourth Military Medical University, 127 Changle West Road, Xi'an 710032, China

[2]Department of Clinical Laboratory, The First Affiliated Hospital of General Hospital of PLA, 28 Fuxing Road, Beijing, 100048, China

[3]Department of Thoracic Surgery, Tangdu Hospital, The Fourth Military Medical University, 1 Xinsi Road, Xi'an 710038, China

[4]Department of Prosthodontics, School of Stomatology, The Fourth Military Medical University, 145 Changle West Road, Xi'an 710032, China

Financial support: This study was supported by grants from the 12th National Five Years Supporting Project of China (2011BAI11B20 to W.X. Duan and 2011BAI11B19 to W.S. Chen), the National Natural Science Foundation of China (81102687 to W.X Duan, 81270170 to S.Q. Yu, 81070198 to S.Q. Yu, and 81000938 to X.L. Yan), the grants from the Excellent Doctoral Support Project of the Fourth Military Medical University (2013D01 to Y. Yang), the Academic Promotion Project of Xijing Hospital (XJZT10 M11 to W.X. Duan) and the Social Development Project of Shaanxi Province (2012JQ4001 to W.X. Duan, 2012K15-02-01 to Z.X. Jin, and 2012SF2-21-1 to Z.X. Jin).

*These authors contributed equally to this work.

#Address correspondence to:

Wensheng Chen, M.D., Ph.D., and Weixun Duan, M.D., Ph.D.

Department of Cardiovascular Surgery

Xijing Hospital

Fourth Military Medical University

127 Changle West Road

Xi'an 710032, China

Tel.: +86 29 84775314

Fax: +86 29 83210092

E-mail address: wenshengchen210@126.com (Wensheng Chen), and weixunduan210@126.com (Weixun Duan)

Author Contributions: Wensheng Chen and Weixun Duan conceived and designed the paper. Zhenxing Liang, Yang Yang, Haibin Wang, and Wei Yi, Xiaolong Yan carried out the experiments and wrote the Paper. Juanjuan Yan, Yue Li, Yingtong Feng, Shiqiang Yu, Jian Yang, and Zhenxiao Jin collected the data.

Conflict of interest: The authors declare that they have no conflicts of interest in the studies described.

Running Title: SIRT1 in the antitumor activity of silybin

Key words: Silybin; Lung adenocarcinoma; SIRT1; p53; Antitumor

Word count (excluding references): 5662

Total number of figures and tables**:** 8 figures

Abstract

Although silybin, a natural flavonolignan, has been shown to exhibit potent antitumor activities against various types of cancers, including lung cancer, the molecular mechanisms behind these activities remain unclear. Silent information regulator 1 (SIRT1) is a conserved nicotinamide adenine dinucleotide (NAD^+)-dependent deacetylase that has been implicated in the modulation of transcriptional silencing and cell survival. Furthermore, it plays a key role in carcinogenesis through the deacetylation of important regulatory proteins, including p53. In this study, we investigated the antitumor activity of silybin towards human lung adenocarcinoma cells in vitro and in vivo and explored the role of the SIRT1 signaling pathway in this process. Silybin treatment resulted in a dose- and time-dependent decrease in lung adenocarcinoma A549 cell viability. Additionally, silybin exhibited strong antitumor activity illustrated by reductions in tumor cell adhesion, migratory capability, and glutathione (GSH) levels and by increased apoptotic indices and reactive oxygen species (ROS) levels. Silybin treatment also downregulated SIRT1 and upregulated p53 acetylation. SIRT1 siRNA (in vitro) or cambinol (a known SIRT1 inhibitor used for in vivo studies) further enhanced the antitumor activity of silybin. In summary, silybin is a potent inhibitor of lung adenocarcinoma cell growth that interferes with SIRT1 signaling, and this inhibition is a novel mechanism of silybin action that may be used for therapeutic intervention in lung adenocarcinoma treatment.

Introduction

Lung cancer is the leading cause of cancer burden worldwide with over 3 million cases and 1 million deaths occurring annually (1). Non-small cell lung cancer (NSCLC) subtypes (adenocarcinoma, squamous cell carcinoma, and large cell carcinoma) account for 80-85% of all lung cancers. The majority of patients with NSCLC are diagnosed during advanced stages and exhibit inoperable local or distant metastases (2). Despite extensive research, the overall 5-year survival rate of lung cancer patients is only 8-14%, and this rate has improved only marginally over the past 30 years (1, 3). These alarming statistics suggest that additional strategies are needed to control this disease.

An essential requirement for any successful long-term cancer chemoprevention strategy is that the chemopreventive agent exhibits little or no toxicity (4). An example of such an agent is silybin (the chemical structure of which is shown in Fig. 1A), a flavanone present in milk thistle (*Silybum marianum L.*) that is used as a hepatoprotective agent and has been marketed as a dietary supplement (5). Silybin exhibits strong chemopreventive and anticancer properties towards various models of colon (6), liver (7), kidney (8), brain (9), prostate, and breast cancer (10), among others. Moreover, no median lethal dose (Lethal Dose, 50%, LD50) for silybin has been reported in laboratory animals, and it has also been considered exceptionally safe due to its extremely low toxicity in both animals and humans during acute or chronic administration; these findings emphasize the importance of utilizing this effective biological agent in cancer chemoprevention studies (1,11). With respect to lung cancer, silybin has been shown to cause significant growth inhibition and apoptosis in both small cell lung cancers and NSCLCs (1, 3, 11). However, the mechanisms responsible for the anti-tumor effects of silybin in lung

adenocarcinoma have not yet been fully elucidated.

Sirtuins are NAD^+-dependent class III histone deacetylases that are conserved from bacteria to eukaryotes (12). Silent information regulator 1 (SIRT1) is the most well-studied family member due to its purported ability to prolong the lifespan of several species including *Drosophila melanogaster*, *Caenorhabditis elegans*, and mammals (12, 13). SIRT1 deacetylates histone proteins and other key transcriptional regulators such as p53, the forkhead box O (FoxO) transcription factors, nuclear factor-κB (NF-κB), liver X receptor (LXR), peroxisome proliferator-activated receptor γ (PPARγ), and the hypoxia-inducible transcription factors (HIFs) (12-14). SIRT1 reportedly performs a wide variety of functions in various biological systems including obesity-associated metabolic diseases, aging, cellular senescence, stress, and inflammation (15). Over the past decade, a controversial view of the role of SIRT1 in tumorigenesis has emerged. SIRT1 was found to be overexpressed in many cancers including prostate, colon, acute myeloid leukemia, and lung cancers (16, 17). Additionally, SIRT1 overexpression in tumor cells correlated with the silencing of tumor suppressor genes (TSGs) and resistance to chemotherapy and ionizing radiation (16, 18). The inhibition of SIRT1 by small molecular inhibitors, dominant negative expression vectors, and small interfering RNA (siRNA) not only rescues TSG expression but also affects key phenotypic aspects of cancer cells (19, 20). Moreover, the pharmacological effects of silybin can be achieved through the regulation of SIRT1 signaling (21-24). In this study, we assess the antitumor activity of silybin towards human lung adenocarcinoma cells and explore the role of SIRT1in silybin activity.

Materials and methods

Materials.

Silybin, SIRT1 siRNA and antibodies against SIRT1 and p53 were obtained from Santa Cruz Biotechnology (Santa Cruz, CA, USA). Cambinol (a SIRT1 inhibitor), dithiothreitol (DTT), 3-(4,5-dimethylthiazol-2-yl)-2, 5-diphenyltetrazolium bromide (MTT), dimethyl sulfoxide (DMSO), and 2',7'-dichlorofluorescein diacetate (2',7'-DCFH-DA) were purchased from Sigma-Aldrich (St. Louis, MO, USA). Antibodies against acetylated-p53 (Lys382), cytochrome c, Bcl2, Bax, and β-actin were purchased from Cell Signaling Technology (Beverly, MA, USA). The fluorescein isothiocyanate (FITC)-Annexin V (AV)/propidium iodide (PI) staining kit and Bradford protein assay kit were purchased from the Beyotime Institute of Biotechnology (Nanjing, Jiangsu, China). The glutathione (GSH) kit was obtained from Cayman Chemical (Ann Arbor, MI, USA). Rabbit anti-goat, goat anti-rabbit and goat anti-mouse secondary antibodies were purchased from the Zhongshan Company (Beijing, China).

Cell culture and treatment.

Human A549 lung adenocarcinoma cells were obtained from the Cell Culture Center at the Chinese Academy of Medical Sciences (Shanghai, China). A quality control including short tandem repeat (STR) analysis was conducted by the provider, and the results of the STR analysis corresponded to the data in American Type Culture Collection (ATCC) cell banks. The cells were grown in Dulbecco's modified Eagle's medium (Gibco, Grand Island, NY, USA) supplemented with 10% fetal bovine serum (Gibco), L-glutamine (2 mM), penicillin (100 units/ml), streptomycin (100 units/ml), and HEPES (25 mM). The cells were maintained in the presence of 5% CO_2 at 37°C. The cells were treated with different concentrations of silybin (originally dissolved in DMSO) for the indicated time periods. An equal amount of DMSO (vehicle) was added to each

treatment including the control. The DMSO concentration did not exceed 0.1% (v/v) for any treatment.

Cell viability assay.

A549 cell viability was assessed via the MTT assay. After treatment, the cells were washed with PBS, and 100 μL of a 0.5 mg/ml MTT solution dissolved in phenol red-free DMEM was added to the cell cultures. The samples were incubated for 4 h at 37°C. Next, 100 μL of DMSO were added to each well, and the samples were shaken for 15 min at 37°C. The absorbance of each well was measured at 490 nm on a SpectraMax 190 spectrophotometer (Molecular Device, Sunnyvale, CA, USA), and cell viability was expressed as an optical density (OD) value.

Analysis of cell apoptosis.

A549 cell apoptosis was detected using the FITC-AV/PI staining kit. Cells were treated with silybin in six-well culture plates (1×10^6 cells/well), trypsinized, counted, washed twice in ice-cold PBS, and resuspended in 1× binding buffer (10 mM HEPES/NaOH, 140 mM NaCl, and 2.5 mM $CaCl_2$, pH 7.4). First, 5 μL of AV (20 μg/mL) and 10 μL of PI (25 μg/mL) were added to 100 μL of the cell suspension followed by incubation for 15 min at room temperature in the dark. Finally, 400 μL of binding buffer were added to each sample, and the samples were kept on ice prior to analysis with a FACScan flow cytometer equipped with the FACStation data management system and Cell Quest software (all from Becton Dickinson, San Jose, CA, USA).

Analysis of intracellular ROS generation.

DCFH-DA passes through cell membranes and is cleaved by esterases to yield DCFH. ROS oxidize DCFH to generate the fluorescent compound dichlorofluorescein which can then be used for quantification of ROS. After treatment with silybin, cells were trypsinized and subsequently

incubated with DCFH-DA (20 μM) in PBS at 37°C for 2 h. After incubation, the DCFH fluorescence of the cells in each well was measured using an FLX 800 microplate fluorescence reader at an excitation wavelength of 485 nm and an emission wavelength of 530 nm (Biotech Instruments Inc., USA). The background was determined by measuring wells that did not contain cells. The fluorescence intensity of the control group was defined as 100%.

Analysis of GSH levels.

GSH levels in the cells were determined using a commercial kit as previously described (19). Briefly, after treatment with silybin, the cells were scraped, collected, and washed with PBS. The resulting cell suspensions were used to determine the GSH levels using the previously mentioned kit according to the manufacturer's instructions. GSH levels were evaluated by comparing samples to the standards and normalizing these values to the total protein content. The results were expressed as total GSH (% of control), and the reduced form of GSH was used as the standard.

Analysis of caspase 3 activity.

Caspase 3 activity was measured with a colorimetric assay kit (MBL International Corporation, Nagoya, Japan) according to the manufacturer's instructions as previously described (25). The cells were washed in ice-cold PBS, and protein was extracted and stored at -80˚C. Cell lysates (20 μl) were added to a buffer containing a p-nitroaniline (pNA)-conjugated substrate for caspase-3 (Ac-DEVD-pNA) in a total reaction volume of 100 μl. Incubations were performed at 37˚C. The released pNA concentrations were calculated from the absorbance values obtained at 405 nm and the calibration curve of the defined pNA solutions. The caspase 3 activity in the control group was set to 100%.

Analysis of cell adhesion.

In our preliminary experiments, we found that silybin (less than 40 μM) treatment for 24 h had no effect on A549 cell proliferation; therefore, we performed adhesion and migration assays after 24 h of silybin treatment (10, 20, and 40 μM). This assay was performed as previously described (19). After treatment with silybin, cells were centrifuged and resuspended in basal medium with 10% fetal bovine serum. The treated cells (1×10^4 cell per well) were placed in a 96-well plate and incubated for 30 min at 37ºC. After the cells were allowed to adhere for 30 min, they were gently washed 3 times with PBS. The adherent cells were stained with MTT and observed under an inverted/phase contrast microscope. Pictures were taken with an Olympus BX61 camera (Japan). Finally, 100 μL of DMSO were added to each well, and the samples were incubated for 15 min at 37°C with constant shaking. The wells were measured by a SpectraMax 190 spectrophotometer at a wavelength of 490 nm (Molecular Device, Sunnyvale, CA, USA), and the OD value of the control group was set to 100%.

Analysis of wound healing.

A cell culture wound-healing assay was performed according to well-established methods (26). The cells were grown to confluence, and a linear wound was created in the confluent monolayer with a 200 μl micropipette tip. The cells were then washed with PBS to eliminate detached cells. After treatment with silybin for 24 h, wound edge movement was monitored under a microscope. The results are expressed as the distance between the cells on each side of the scratch wound.

Small interfering RNA transfection.

A549 cells were plated into 6-, 24-, or 96-well plates at a subconfluent density. The cells were transiently transfected with negative control siRNA or SIRT1 siRNA at a concentration of 50 pM for 48 h with the Lipofectamine RNAiMAX reagent (Invitrogen, Carlsbad, CA, USA) in

OPTI-MEM media (Gibco, Carlsbad, CA, USA). The cells were subsequently prepared for further experiments.

Extraction of cytosolic cytochrome c

Extraction of cytosolic cytochrome c was performed as previously described (26). After treatment, the cells were harvested by centrifugation at 1,000 rpm for 5 min. The pellets were washed twice with ice-cold PBS, re-suspended in a 5-fold volume of ice-cold cell extract buffer [20 mM 4-(2-hydroxyethy1)-1-piperazineethanesulfonic acid (HEPES-KOH; pH7.5), 10 mM KCl, 1.5 mM MgCl2, 1 mM ethylene diamine tetraacetic acid (EDTA), 1 mM ethylene glycol tetraacetic acid (EGTA), 1 mM DTT, 250 mM sucrose, 0.1 mM phenylmethylsulfonyl fluoride, and 0.02 mM aprotinin] and incubated for 40 min at 4 ºC. Then, the cells were centrifuged at 1,200 rpm for 10 min at 4 ºC, and the final supernatant containing the cytosolic fraction of cytochrome c was used for Western blot analyses.

Antitumor activity in a xenograft model.

Male athymic nude mice were purchased from the Laboratory Animal Centre of the Fourth Military Medical University. The mice were housed and maintained under specific pathogen-free conditions in facilities approved by the American Association for the Accreditation of Laboratory Animal Care and in accordance with the current regulations and standards of the United States Department of Agriculture, United States Department of Health and Human Services. The present study was performed according to the Guide for the Care and Use of Laboratory Animals, published by the US National Institutes of Health (National Institutes of Health Publication No. 85-23, revised 1996) and was approved by the Ethics Committee of the Fourth Military Medical University. All surgeries were performed under sodium pentobarbital anesthesia, and all efforts

were made to minimize animal suffering. As described in our previous study (2), A549 cell tumor xenografts were established by subcutaneously injecting 1×10^6 cells into the right flanks of 4 to 6-week-old male athymic nude mice. Based on the data obtained from a pilot study, we initiated treatment when the tumor volumes reached approximately 100 mm^3. The tumor volumes (V) were calculated using the following formula: $V = A \times B^2/2$ (A = largest diameter; B = smallest diameter). First, the mice were randomly divided into 3 groups (n= 6 per group): control (saline) and silybin suspended in saline at either 250 or 500 mg/kg body weight; silybin was administered 5 days/week by oral gavage. Next, the mice were randomly divided into control, silybin, cambinol+silybin, and cambinol groups (n=6). Silybin was orally administered to the mice at doses of 500 mg/kg body weight per day (5 days/week), cambinol (50 mg/kg) or control (0.05% DMSO), all of which were diluted with saline and administered intraperitoneally (5 days/week). The body weight and tumor sizes were measured every 3 days with calipers (days 2, 5, 8, 11, 14, 17, and 20). On day 20, the tumors were excised from the euthanized mice for Western blot analysis.

Analysis of experimental lung metastasis in vivo

Male NOD/SCID mice (5-weeks) were purchased from the Vital River Company (Beijing, China) and treated similar to the athymic nude mice before experiments were performed. A549 cells (1×10^6 cells in 0.2 ml PBS) were injected into the tail veins of the mice. Then, the mice were randomly divided into four groups upon induction of metastasis including control, silybin, cambinol+silybin, and cambinol groups (n=6). The concentrations and administration of silybin and cambinol were the same as those used in the xenograft experiments described above. The mice were sacrificed 6 weeks after injection and the lungs were dissected out and photographed.

Visible A549 colonies on the surface of the lung were counted.

Western blot analyses.

The cell, cell cytosolic fraction, and tumor tissue samples were homogenized in lysis buffer containing a 1% protease inhibitor cocktail. The lysates were centrifuged for 15 min at 12,000 rpm, and the resulting supernatants were transferred to new tubes and stored at -70 °C. The protein concentrations were determined with a Bradford protein assay kit. Proteins were separated by electrophoresis and transferred to nitrocellulose membranes. The membranes were blocked for 1 h in Tris-buffered saline and Tween-20 (TBST, pH 7.6) containing 5% non-fat dry milk and were then incubated overnight at 4 °C with antibodies against SIRT1, p53 (1:500 dilution), acetylated-p53, cytochrome c, Bcl2, Bax, and β-actin (1:1000 dilution) followed by several TBST washes. The membranes were then probed with the appropriate secondary antibodies (1:5000 dilution) at room temperature for 90 min and washed with TBST. The protein bands were detected with a Bio-Rad imaging system (Bio-Rad, Hercules, CA, USA) and quantified with the Quantity One software package (West Berkeley, CA, USA).

Statistical analysis.

All values are presented as the mean ± standard deviation (SD). Group comparisons were performed by ANOVA (SPSS 13.0). All of the groups were analyzed simultaneously with an LSD *t* test. A difference of $P<0.05$ was considered statistically significant.

Results

Effects of silybin on lung adenocarcinoma cell viability and apoptosis

The viability of silybin-treated A549 cells was determined by the MTT assay, and the data are presented in Fig. 1B. The treatment of A549 cells for 12, 24, or 36 h with 100, 200, or 400 μM of silybin demonstrated inhibition of cell growth in a dose- and time-dependent manner. The microscopy images (Fig. 1C) show that silybin treatment resulted in significant cell shrinkage and a decrease in the rate of cellular attachment when compared to the control treatment. After treatment with 100, 200, or 400 μM of silybin for 24 h, the apoptotic index increased in a dose-dependent manner ($P<0.01$when compared to the control group). These results provide convincing data indicating that silybin can induce A549 cell apoptosis (Fig. 1D).

Effects of silybin on ROS generation, GSH levels and caspase 3 activity in lung adenocarcinoma cells

To determine whether silybin causes intracellular oxidation, we used the specific oxidation-sensitive fluorescent dye DCFH-DA, which exhibits enhanced fluorescence intensity following the generation of intracellular reactive metabolites. Silybin treatment for 24 h induced dose-dependent ROS generation in A549 cells ($P<0.01$ when compared to the control group; Fig. 2A). Reduced GSH is the major non-protein thiol present in cells, and it is essential for the maintenance of cellular redox status. Because silybin-induced apoptosis in A549 cells correlated with ROS generation, we hypothesized that silybin treatment may disturb the cellular redox status. To address this issue, we determined the effects of silybin treatment on intracellular GSH levels. After treatment with silybin (24 h), we observed a dose-dependent decrease in intracellular GSH levels in A549 cells ($P<0.01$ when compared to the control group; Fig. 2B). Furthermore, we also found that silybin treatment led to higher levels of caspase 3 activity (Fig. 2C).

Effects of silybin on lung adenocarcinoma cell migration and adhesion

After a 24 h incubation with silybin, the cell adhesion ratio decreased significantly ($P<0.01$ when compared to the control group; Fig. 3A), and the effects of silybin on cell adhesion and migratory capability were dose-dependent. Additionally, the distances between the scratch wounds were longer in the silybin treated group, and the migratory distance of the cells was reduced by silybin treatment ($P<0.01$ when compared to the control group; Fig. 3B). These results indicate that silybin reduces cell adhesion and the migratory capability of A549 cells.

Effects of silybin on SIRT1 pathway and mitochondrial apoptotic pathway-related proteins in lung adenocarcinoma cells

Silybin treatment for 24 h induced a dose-dependent downregulation of SIRT1 and an upregulation of acetylated-p53 ($P<0.01$ when compared to the control group; Fig. 4). Additionally, the mitochondrial apoptotic pathway-related proteins Bax and cytosolic cytochrome c were upregulated by silybin treatment; in contrast, Bcl2 was downregulated ($P<0.01$ when compared to the control group; Fig. 4).

Effects of silybin combined with SIRT1 siRNA on cell viability and SIRT1 signaling in lung adenocarcinoma cells

SIRT1 siRNA significantly decreased SIRT1 levels and increased acetylated-p53 expression in A549 cells ($P<0.01$ when compared to the control siRNA group; Fig. 5B). SIRT1 siRNA also slightly decreased the viability of A549 cells; however, this difference was not significant ($P>0.05$ when compared to the control siRNA group; Fig. 5A). The combination of SIRT1 siRNA and silybin (200 μM) significantly decreased cell viability ($P<0.01$ when compared to both the silybin and SIRT1 siRNA groups; Fig. 5A). Additionally, Bax and cytosolic cytochrome c were further

upregulated by silybin and SIRT1 siRNA co-treatment, whereas Bcl2 was further downregulated ($P<0.01$ when compared to the silybin and SIRT1 siRNA groups; Fig. 5B).

Effects of silybin on tumor xenografts in vivo

To determine whether silybin could inhibit tumor growth in animals, we established A549 xenografts in athymic nude mice. We found that the mice in all treatment groups developed subcutaneous tumors. As shown in Figures 6A and 6B, silybin treatment (250 or 500 mg/kg) significantly inhibited tumor growth ($P<0.01$ when compared to the control group). Silybin treatment (250 or 500 mg/kg) did not cause death or abnormal behavior and did not affect body weight gain ($P>0.05$ when compared to the control group; Fig. 6C). Western blot analysis showed that silybin treatment induced a dose-dependent downregulation of SIRT1 and upregulated the acetylation of p53 ($P<0.01$ when compared to the control group; Fig. 6D). Additionally, the mitochondrial apoptotic pathway-related protein Bax was upregulated by silybin treatment, whereas Bcl2 was downregulated ($P<0.01$ when compared to the control group; Fig. 6D).

Effects of silybin combined with cambinol on tumor xenografts in vivo

As shown in Figures 7A and 7B, treatment with silybin or cambinol alone significantly inhibited tumor growth ($P<0.01$ or $P<0.05$ when compared to the control group, respectively). The combination of silybin and cambinol further inhibited tumor growth ($P<0.01$ when compared to the silybin or cambinol groups). Silybin or cambinol treatment did not affect animal body weight ($P>0.05$ when compared to the control group; Fig. 7C).Western blot analysis showed that silybin and cambinol co-treatment further decreased SIRT1 levels and increased acetylated-p53 expression ($P<0.01$ when compared to the silybin and cambinol groups; Fig. 7C). Additionally,

Bax was further upregulated by silybin and cambinol co-treatment, whereas Bcl2 was further downregulated ($P<0.01$ when compared to the silybin and cambinol groups; Fig. 7C).

Effects of combination silybin and cambinol treatment on tumor pulmonary metastasis in vivo

NOD/SCID micewere used to explore the effects of combined silybin and cambinol treatment on tumor pulmonary metastasis. As shown in Figures 8A and 8B, treatment with silybin alone significantly decreased pulmonary metastatic colonies ($P<0.01$ when compared to the control group). The combination of silybin and cambinol further decreased pulmonary metastatic colonies ($P<0.01$ when compared to the silybin or cambinol groups). Treatment with cambinol alone slightly decreased pulmonary metastatic colonies ($P<0.05$ when compared to the control group).

Discussion

There is increasing evidence that nutraceutical agents are important for cancer prevention and intervention (1, 11, 27) because dietary and non-dietary agents and lifestyle determine cancer incidence and may also affect the growth, progression or aggressiveness of cancer cells (27). Silybin is a flavonolignan and the major active constituent of silymarin, which is a complex mixture of flavonolignans and polyphenols that are extracted from milk thistle seeds. The German Commission E has recommended its use for dyspeptic complaints and liver conditions including toxin-induced liver damage and hepatic cirrhosis. It has also been recommended as a supportive therapy for chronic inflammatory liver conditions (28). Neither milk thistle extract nor silybin is currently approved for any medical use in the USA; however, it is sold as a dietary supplement and is one of the most frequently sold herbal products in the USA (28). The anticancer efficacy of

silybin is clearly evident in the published reports of its effects against various cancers generated over the last two decades; these effects mainly target proliferation, apoptosis, inflammation, angiogenesis, and cancer cell metabolism (6-10). Various molecules and signaling pathways are involved in the anti-tumor effects of silybin including vascular endothelial growth factor (VEGF), VEGF receptors, inducible nitric oxide synthase (iNOS), signal transducers, activators of transcription (STATs), PI3K/Akt, β-catenin, IGF-IGFBP3, nuclear factor kappa B (NF-κB), and mitogen-activated protein kinases (MAPKs) (3-12,27). However, the effects of silybin on human lung adenocarcinoma and the mechanisms responsible for these effects are not fully understood. In our study, silybin treatment resulted in a dose- and time-dependent inhibition of cell viability and the induction of apoptosis in A549 lung adenocarcinoma cells. Silybin also significantly blocked lung adenocarcinoma cell adhesion and migration, both of which are major events that determine the metastatic potential of tumors. Additionally, silybin treatment significantly inhibited tumor growth in A549 xenografts in athymic nude mice and decreased the number of pulmonary metastatic colonies found in NOD/SCID mice.

SIRT1 is a conserved NAD^+-dependent deacetylase that has been implicated in the modulation of transcriptional silencing and cell survival. It also plays a key role in carcinogenesis through the deacetylation of important regulatory proteins (19). SIRT1 is highly expressed in several human cancers including lung, colon, breast, liver, and prostate cancers (29-31). Studies have also shown that the inhibition of SIRT1 expression and/or activity by siRNA or small molecular inhibitors promoted cell cycle arrest and induced apoptosis in cancer cells (29, 32). Moreover, the pharmacological effects of silybin can be achieved through the regulation of SIRT1 signaling (21-24). For example, by promoting SIRT1 expression and recovering the physiologically

autophagic cells, silybin could reverse hyperglycemia and repair damaged pancreatic β-cells (22). Silybin exhibits protective effects against isoproterenol-induced rat cardiac myocyte injury after SIRT1 upregulation (23, 24). Importantly, Wang and colleagues have shown that silybin-induced apoptosis was significantly reinforced by blocking insulin-like growth factor 1 receptor (IGF-1R) signaling with tyrphostin AG1024, a specific inhibitor of IGF-1R autophosphorylation. The downregulation of SIRT1 expression was apparently enhanced by AG1024 in silybin-treated MCF-7 breast cancer cells (21).

The vital importance of the tumor suppressor gene p53 in the prevention of human cancer development and progression is demonstrated by the fact that p53 mutations are detected in 50% of all human cancers and is also emphasized by accumulating evidence that p53 protein function and stability are often abrogated via posttranslational mechanisms in the remaining human cancers that express wild-type p53 (29). Cancers must frequently disarm p53; once p53 is activated, it triggers cell growth arrest, apoptosis, autophagy, or senescence, all of which are detrimental to cancer cells. Furthermore, p53 impedes cell migration, metabolism, and angiogenesis, which are favorable conditions for cancer cell progression and metastasis (29, 33). A variety of posttranslational modifications can regulate p53 activity including phosphorylation, acetylation, methylation, and sumoylation, and these modifications have been previously described (34, 35). Acetylation reportedly plays an important role in p53 stabilization, nuclear localization and transcriptional activation and can lead to p53 activation in a manner independent of its phosphorylation status (34, 36). SIRT1 can deacetylate several lysine residues in the p53 protein (34). Cambinol is a cell permeable naphthol compound that inhibits the NAD+-dependent deacetylase activities of SIRT1 and SIRT2 (IC50 = 56 mM and 59 mM, respectively) and does not

inhibit class I or II histone deacetylase activity (37, 38). Unlike sirtinol (a known SIRT1 inhibitor), cambinol can be used in vivo and was shown to effectively inhibit Bcl6-expressing Burkitt's lymphoma xenograft growth in mice (38). A previous study has verified that the use of a 100 mg/kg cambinol dose had no toxic effects on the animals which displayed no weight loss or increases in serum transaminase levels (37). In this study, we found that silybin treatment inhibited SIRT1 and activated acetylated-p53 in A549 cells. When combined with SIRT1 siRNA in vitro or cambinol in vivo, silybin further decreased the viability of lung adenocarcinoma cells, inhibited tumor growth, and decreased the number of pulmonary metastatic colonies. As expected, we observed that A549 cells treated with SIRT1 siRNA or cambinol exhibited increased p53 acetylation when also treated with silybin. These results suggest that SIRT1 downregulation enhances the effects of silybin in part by increasing p53 acetylation.

GSH is a major cellular non-protein antioxidant that eliminates $O_2^{\bullet-}$ and provides electrons for enzymes such as GSH peroxidase which reduces H_2O_2 to H_2O. Reports have indicated that the intracellular GSH content exhibits a decisive effect on anticancer drug-induced apoptosis suggesting that apoptotic effects are inversely correlated with GSH content. Reduced GSH is the major non-protein thiol present in cells and is essential for the maintenance of cellular redox status (19). A majority of chemotherapeutic drugs inhibit cancer cell viability and induce apoptosis through the intrinsic mitochondrial apoptotic pathway; important members of this pathway includeBcl2, Bax, and cytochrome c (39). Release of cytochrome c from mitochondria is a hallmark of apoptosis [26]. Studies have provided novel evidence that SIRT1 may be involved in the intrinsic mitochondrial apoptotic pathway (40). During apoptosis, mitochondria serve as a source of ROS, and enhanced ROS production is related to the apoptotic responses induced by

antitumor agents (39). Our results show that silybin treatment depletes intracellular GSH levels and increases ROS production in A549 cells. Moreover, in addition to downregulating SIRT1 signaling, silybin also increased intracellular caspase 3 activity, upregulated Bax and cytosolic cytochrome c protein levels, and downregulated Bcl2 protein levels. These findings verify previous work in which the inhibition of SIRT1 signaling was associated with the induction of the mitochondrial apoptotic pathway in human cancer cells (41).

In conclusion, these experiments provide mechanistic evidence that silybin treatment inhibits lung adenocarcinoma cell growth and metastasis via the downregulation of SIRT1 signaling. Furthermore, the downregulation of SIRT1 signaling sensitizes lung adenocarcinoma cells to silybin treatment. Therefore, silybin has multiple advantages that make it a strong candidate for therapeutic applications in lung adenocarcinoma, and SIRT1 downregulation appears to be an effective gene therapy strategy for the treatment of cancer.

References

1. Chittezhath M, Deep G, Singh RP, Agarwal C, Agarwal R. Silibinin inhibits cytokine-induced signaling cascades and down-regulates inducible nitric oxide synthase in human lung carcinoma A549 cells. Mol Cancer Ther 2008;7:1817-26.
2. Yang Y, Yan X, Duan W, Yan J, Yi W, Liang Z, et al. Pterostilbene exerts antitumor activity via the Notch1 signaling pathway in human lung adenocarcinoma cells. PLoS One 2013;8:e62652.
3. Tyagi A, Singh RP, Ramasamy K, Raina K, Redente EF, Dwyer-Nield LD, et al. Growth inhibition and regression of lung tumors by silibinin: modulation of angiogenesis by

macrophage-associated cytokines and nuclear factor-kappaB and signal transducers and activators of transcription 3. Cancer Prev Res (Phila) 2009;2:74-83.

4. Singh RP, Deep G, Chittezhath M, Kaur M, Dwyer-Nield LD, Malkinson AM, et al. Effect of silibinin on the growth and progression of primary lung tumors in mice. J Natl Cancer Inst 2006;98:846-55.

5. Wu JW, Lin LC, Tsai TH. Drug-drug interactions of silymarin on the perspective of pharmacokinetics. J Ethnopharmacol 2009;121:185-93.

6. Lin CM, Chen YH, Ma HP, Wang BW, Chiu JH, Chua SK, et al. Silibinin inhibits the invasion of IL-6-stimulated colon cancer cells via selective JNK/AP-1/MMP-2 modulation in vitro. J Agric Food Chem 2012;60:12451-7.

7. Brandon-Warner E, Eheim AL, Foureau DM, Walling TL, Schrum LW, McKillop IH. Silibinin (Milk Thistle) potentiates ethanol-dependent hepatocellular carcinoma progression in male mice. Cancer Lett 2012;326:88-95.

8. Liang L, Li L, Zeng J, Gao Y, Chen YL, Wang ZQ, et al. Inhibitory effect of silibinin on EGFR signal-induced renal cell carcinoma progression via suppression of the EGFR/MMP-9 signaling pathway. Oncol Rep 2012;28:999-1005.

9. Yousefi M, Ghaffari SH, Soltani BM, Nafissi S, Momeny M, Zekri A, et al. Therapeutic efficacy of silibinin on human neuroblastoma cells: Akt and NF-κB expressions may play an important role in silibinin-induced response. Neurochem Res 2012;37:2053-63.

10. Lu W, Lin C, King TD, Chen H, Reynolds RC, Li Y. Silibinin inhibits Wnt/β-catenin signaling by suppressing Wnt co-receptor LRP6 expression in human prostate and breast cancer cells. Cell Signal 2012;24:2291-6.

11. Mateen S, Tyagi A, Agarwal C, Singh RP, Agarwal R. Silibinin inhibits human nonsmall cell lung cancer cell growth through cell-cycle arrest by modulating expression and function of key cell-cycle regulators. Mol Carcinog 2010;49:247-58.

12. Wang HJ, Tashiro S, Onodera S, Ikejima T. Inhibition of insulin-like growth factor 1 receptor signaling enhanced silibinin-induced activation of death receptor and mitochondrial apoptotic pathways in human breast cancer MCF-7 cells. J Pharmacol Sci 2008;107:260-9.

13. Corbi G, Conti V, Scapagnini G, Filippelli A, Ferrara N. Role of sirtuins, calorie restriction and physical activity in aging. Front Biosci (Elite Ed) 2012;4:768-78.

14. Rahman S, Islam R. Mammalian Sirt1: insights on its biological functions. Cell Commun Signal 2011;9:11.

15. Haigis MC, Sinclair DA. Mammalian sirtuins: biological insights and disease relevance. Annu Rev Pathol 2010;5:253-95.

16. Martinez-Pastor B, Mostoslavsky R. Sirtuins, metabolism, and cancer. Front Pharmacol 2012;3:22.

17. Roth M, Chen WY. Sorting out functions of sirtuins in cancer. Oncogene 2013. doi: 10.1038/onc.2013.120. [Epub ahead of print]

18. Kalle AM, Mallika A, Badiger J, Alinakhi, Talukdar P, Sachchidanand. Inhibition of SIRT1 by a small molecule induces apoptosis in breast cancer cells. Biochem Biophys Res Commun 2010;401:13-9.

19. Cheng Y, Cai L, Jiang P, Wang J, Gao C, Feng H, et al. SIRT1 inhibition by melatonin exerts antitumor activity in human osteosarcoma cells. Eur J Pharmacol 2013;715:219-29.

20. Pruitt K, Zinn RL, Ohm JE, McGarvey KM, Kang SH, Watkins DN, et al. Inhibition of

SIRT1 reactivates silenced cancer genes without loss of promoter DNA hypermethylation. PLoS Genet 2006;2:e40.

21. Wang HJ, Tashiro S, Onodera S, Ikejima T. Inhibition of insulin-like growth factor 1 receptor signaling enhanced silibinin-induced activation of death receptor and mitochondrial apoptotic pathways in human breast cancer MCF-7 cells. J Pharmacol Sci 2008;107:260-9.

22. Wang Q, Liu M, Liu WW, Hao WB, Tashiro S, Onodera S, et al. In vivo recovery effect of silibinin treatment on streptozotocin-induced diabetic mice is associated with the modulations of Sirt-1 expression and autophagy in pancreatic β-cell. J Asian Nat Prod Res 2012;14:413-23.

23. Zhou B, Wu LJ, Li LH, Tashiro S, Onodera S, Uchiumi F, et al. Silibinin protects against isoproterenol-induced rat cardiac myocyte injury through mitochondrial pathway after up-regulation of SIRT1. J Pharmacol Sci 2006;102:387-95.

24. Zhou B, Wu LJ, Tashiro S, Onodera S, Uchiumi F, Ikejima T. Silibinin protects rat cardiac myocyte from isoproterenol-induced DNA damage independent on regulation of cell cycle. Biol Pharm Bull 2006;29:1900-5.

25. Kauntz H, Bousserouel S, Gosse F, Marescaux J, Raul F. Silibinin, a natural flavonoid, modulates the early expression of chemoprevention biomarkers in a preclinical model of colon carcinogenesis. Int J Oncol 2012;41:849-54.

26. Liu Y, Wang L, Wu Y, Lv C, Li X, Cao X, et al. Pterostilbene exerts antitumor activity against human osteosarcoma cells by inhibiting the JAK2/STAT3 signaling pathway. Toxicology 2013;304:120-31.

27. Deep G, Agarwal R. Antimetastatic efficacy of silibinin: molecular mechanisms and

therapeutic potential against cancer. Cancer Metastasis Rev 2010;29:447-63.

28. Post-White J, Ladas EJ, Kelly KM. Advances in the use of milk thistle (Silybum marianum). Integr Cancer Ther 2007;6:104-9.

29. Zhang Q, Zeng SX, Zhang Y, Zhang Y, Ding D, Ye Q, et al. A small molecule Inauhzin inhibits SIRT1 activity and suppresses tumour growth through activation of p53. EMBO Mol Med 2012;4:298-312.

30. Suzuki K, Hayashi R, Ichikawa T, Imanishi S, Yamada T, Inomata M, et al. SRT1720, a SIRT1 activator, promotes tumor cell migration, and lung metastasis of breast cancer in mice. Oncol Rep 2012;27:1726-32.

31. Holloway KR, Barbieri A, Malyarchuk S, Saxena M, Nedeljkovic-Kurepa A, Cameron Mehl M, et al. SIRT1 positively regulates breast cancer associated human aromatase (CYP19A1) expression. Mol Endocrinol 2013;27:480-90.

32. Dixit D, Sharma V, Ghosh S, Mehta VS, Sen E. Inhibition of Casein kinase-2 induces p53-dependent cell cycle arrest and sensitizes glioblastoma cells to tumor necrosis factor (TNFα)-induced apoptosis through SIRT1 inhibition. Cell Death Dis 2012;3:e271.

33. Vousden KH, Prives C. Blinded by the Light: The Growing Complexity of p53. Cell 2009;137:413-31.

34. Li L, Wang L, Li L, Wang Z, Ho Y, McDonald T, et al. Activation of p53 by SIRT1 inhibition enhances elimination of CML leukemia stem cells in combination with imatinib. Cancer Cell 2012;21:266-81.

35. Vousden KH, Lane DP. p53 in health and disease. Nat Rev Mol Cell Biol 2007;8:275-83.

36. Tang Y, Zhao W, Chen Y, Zhao Y, Gu W. Acetylation is indispensable for p53 activation.

Cell 2008;133:612-26.

37. Laemmle A, Lechleiter A, Roh V, Schwarz C, Portmann S, Furer C, et al. Inhibition of SIRT1 impairs the accumulation and transcriptional activity of HIF-1α protein under hypoxic conditions. PLoS One 2012;7:e33433.

38. Heltweg B, Gatbonton T, Schuler AD, Posakony J, Li H, Goehle S, et al. Antitumor activity of a small-molecule inhibitor of human silent information regulator 2 enzymes. Cancer Res 2006;66:4368-77.

39. Nguyen KC, Willmore WG, Tayabali AF. Cadmium telluride quantum dots cause oxidative stress leading to extrinsic and intrinsic apoptosis in hepatocellular carcinoma HepG2 cells. Toxicology 2013;306:114-23.

40. Adlakha YK, Saini N. miR-128 exerts pro-apoptotic effect in a p53 transcription-dependent and -independent manner via PUMA-Bak axis. Cell Death Dis 2013;4:e542.

41. Kang N, Zhang JH, Qiu F, Tashiro S, Onodera S, Ikejima T. Inhibition of EGFR signaling augments oridonin-induced apoptosis in human laryngeal cancer cells via enhancing oxidative stress coincident with activation of both the intrinsic and extrinsic apoptotic pathways. Cancer Lett 2010;294:147-58.

Figure Legends

Fig. 1 The effects of silybin on the viability, morphology and apoptotic rates of lung adenocarcinoma cells. **A.** The chemical structure of silybin. **B.** Cells were treated with silybin at different concentrations (100, 200 and 400 μM) and time points (12, 24, and 36 h). Viability is expressed as OD values. **C.** Cell morphology was observed under an inverted/phase contrast

microscope (treated for 24 h), and images were obtained. Significant cell shrinkage and a decreased cellular attachment rates were observed in the silybin-treated group. **D.** Representative flow cytometry apoptosis results are shown. Four subpopulations and their fractions are indicated: normal cells (lower left), dead cells (upper left), early apoptotic cells (lower right), and late apoptotic cells (upper right). The apoptotic index is expressed as the number of apoptotic cells/the total number of counted cells × 100%. The results are expressed as the means ± SD, n=6. **P<0.01 when compared to the control group; $^{\#\#}$P<0.01 when compared to the 100 μM silybin group; and $^{\$\$}$P<0.01 when compared to the 200 μM silybin group. SIL, silybin; OD, optical density.

Fig. 2 The effects of silybin on ROS generation, GSH levels, and caspase 3 activity in lung adenocarcinoma cells (24 h). **A.** The ROS concentrations are shown, and the fluorescence intensity of the control group was defined as 100%. **B.** The intracellular GSH levels are shown, and the GSH levels of the control group were defined as 100%. **C.** The intracellular caspase 3 activity levels are shown, and the caspase 3 activity level of the control group was defined as 100%. The results are expressed as the means ± SD, n=6. **P<0.01 when compared to the control group; $^{\#\#}$P<0.01 when compared to the 100 μM silybin group; and $^{\$\$}$P<0.01 when compared to the 200 μM silybin group. SIL, silybin.

Fig. 3 The effects of silybin on adhesion and migration in lung adenocarcinoma cells (24 h). **A.** Representative images of adhesion are shown. The cell adhesion capability is expressed as an adhesion ratio. The number of adherent cells in the control group was set to 100%. **B.** Representative images of wound healing are shown. The migratory capability is expressed as the

mean distance between the two sides of the scratch wound. The mean distance in the control group was set to 100%. The results are expressed as the means ± SD, n=6. **P<0.01 when compared to the control group; $^{\#\#}$P<0.01 when compared to the 10 μM silybin group; and $^{\$\$}$P<0.01 when compared to the 20 μM silybin group. SIL, silybin.

Fig. 4 Effects of silybin on the SIRT1 pathway and mitochondrial apoptotic pathway-related proteins in lung adenocarcinoma cells (24 h). Representative Western blot results are shown. Silybin treatment inhibited SIRT1 expression and Bcl2; it increased p53, acetylated-p53, cytosolic cytochrome c, and Bax expression. The results are expressed as the means ± SD, n=6. **P<0.01 when compared to the control group; $^{\#\#}$P<0.01 when compared to the 100 μM silybin group; and $^{\$\$}$P<0.01 when compared to the 200 μM silybin group. SIL, silybin.

Fig. 5 Effects of combined silybin and SIRT1 siRNA on cell viability and SIRT1 signaling in lung adenocarcinoma cells (24 h). **A.** Viability is expressed as OD values. The combination of silybin and SIRT1 siRNA further inhibited the viability of A549 cells. **B.** Representative Western blot results are shown. The results are expressed as the means ± SD, n=6. **P<0.01 when compared to the control group; $^{\#\#}$P<0.01 when compared to the 200 μM silybin group, and $^{\$\$}$P<0.01when compared to the SIRT1 siRNA + 200 μM silybin group. SIL, silybin; OD, optical density.

Fig. 6 Effects of silybin on A549 tumor xenografts in vivo. **A.** Photographs showing the tumor xenograft morphologies of the various groups. **B.** The tumor growth curve was drawn from the tumor volumes and the treatment duration. **C.** The body weight curve graph is shown for

thetreatment duration. **D.** Representative Western blot results are shown. The results are expressed as the means ± SD, n=6, **P<0.01 when compared to the control group; $^{\#\#}$P<0.01when compared to the 250 mg/kg silybin group. SIL, silybin.

Fig. 7 The effects of combination silybin and cambinol treatment on A549 tumor xenografts in vivo. **A.** Photographs showing the tumor xenograft morphologies for the different groups. **B.** The tumor growth curve was drawn from the tumor volumes and the treatment duration. **C.** The body weight curve graph is shown in for the treatment duration. **D.** Representative Western blot results are shown. The results are expressed as the mean ± SD, n=6. **P<0.01 when compared to the control group; *P<0.05 when compared to the control group; $^{\#\#}$P<0.01 when compared to the 500 mg/kg silybin group; $^{\$\$}$P<0.01 when compared to the cambinol + 500 mg/kg silybin group. SIL, silybin.

Fig. 8 The effects of combination silybin and cambinol treatment on tumor pulmonary metastasis in vivo. **A.** Photographs showing the pulmonary metastatic colony morphologies for the different groups. **B.** The statistical analysis graph of pulmonary metastatic colonies. The results are expressed as the mean ± SD, n=6. **P<0.01 when compared to the control group; *P<0.05 when compared to the control group; $^{\#}$P<0.05when compared to the 500 mg/kg silybin group; $^{\$\$}$P<0.01 when compared to the cambinol + 500 mg/kg silybin group. SIL, silybin.

Figure 1

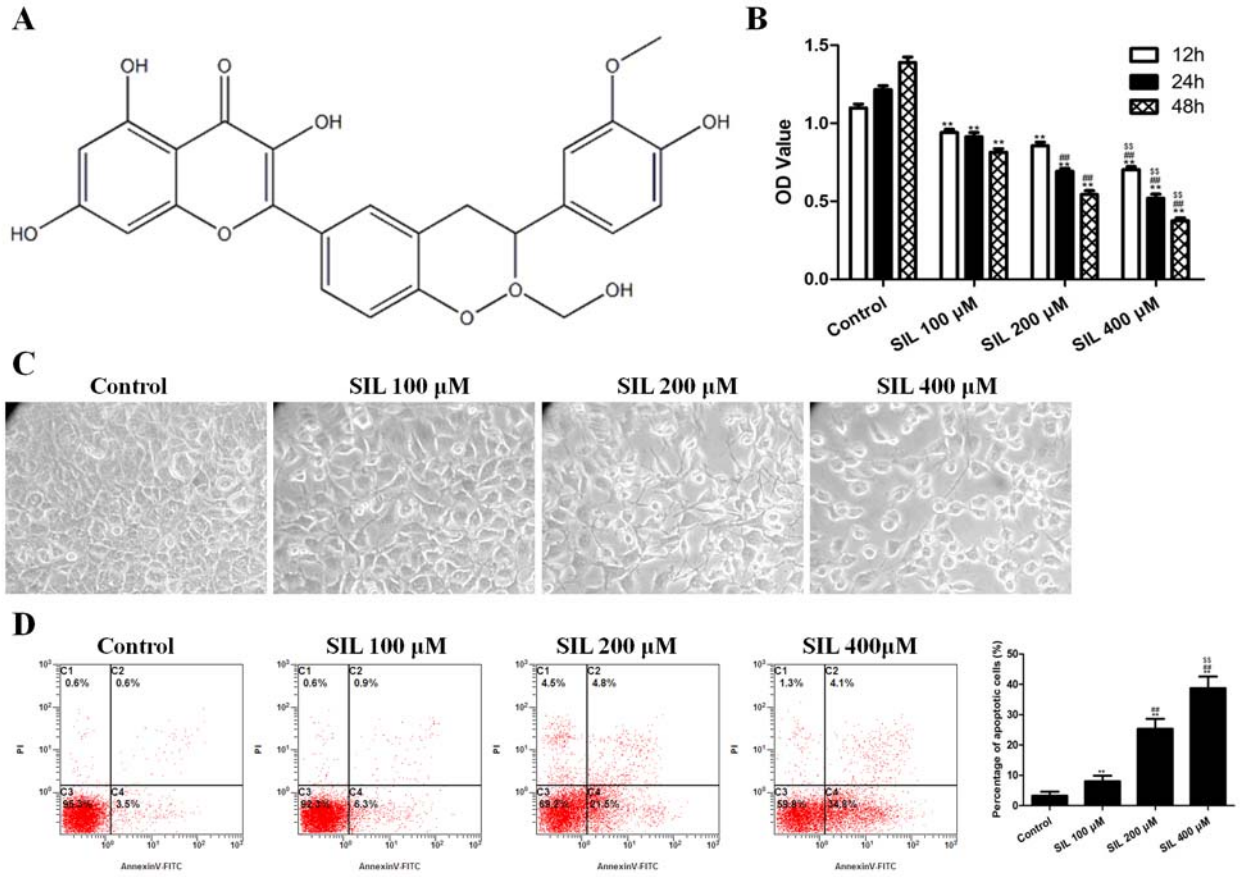

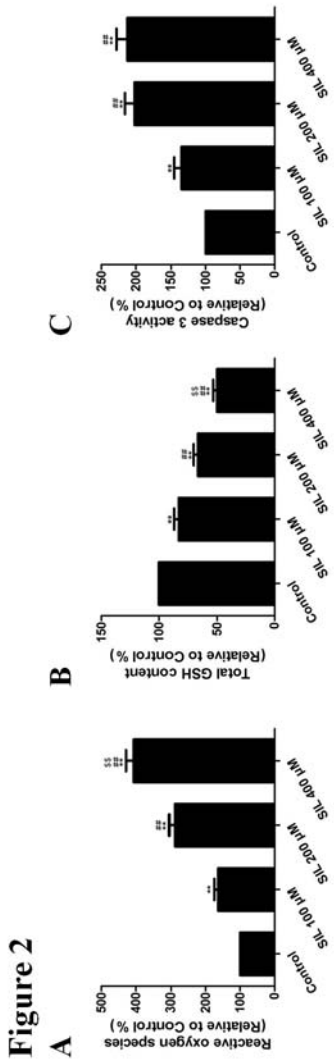

Figure 2

Figure 3

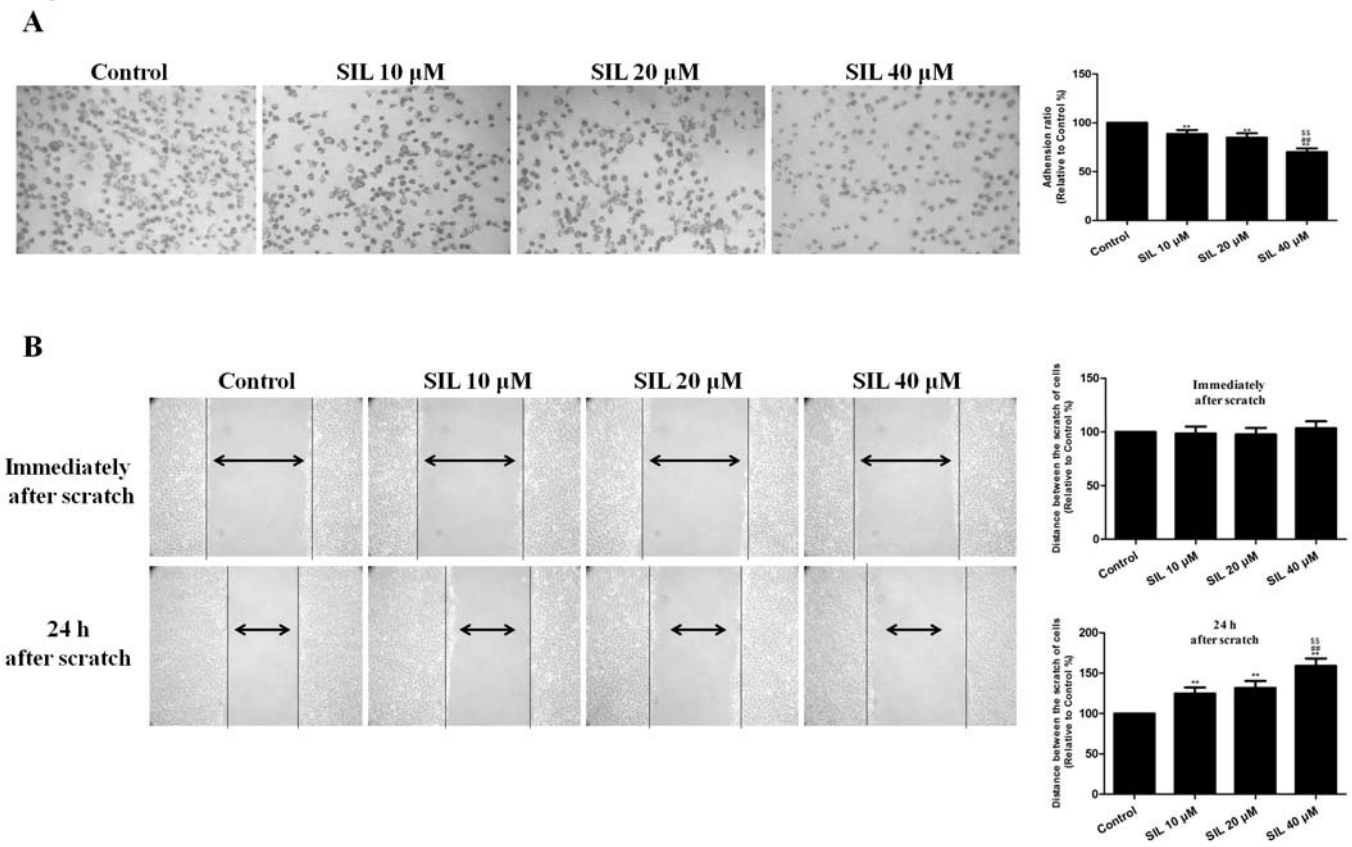

Figure 4

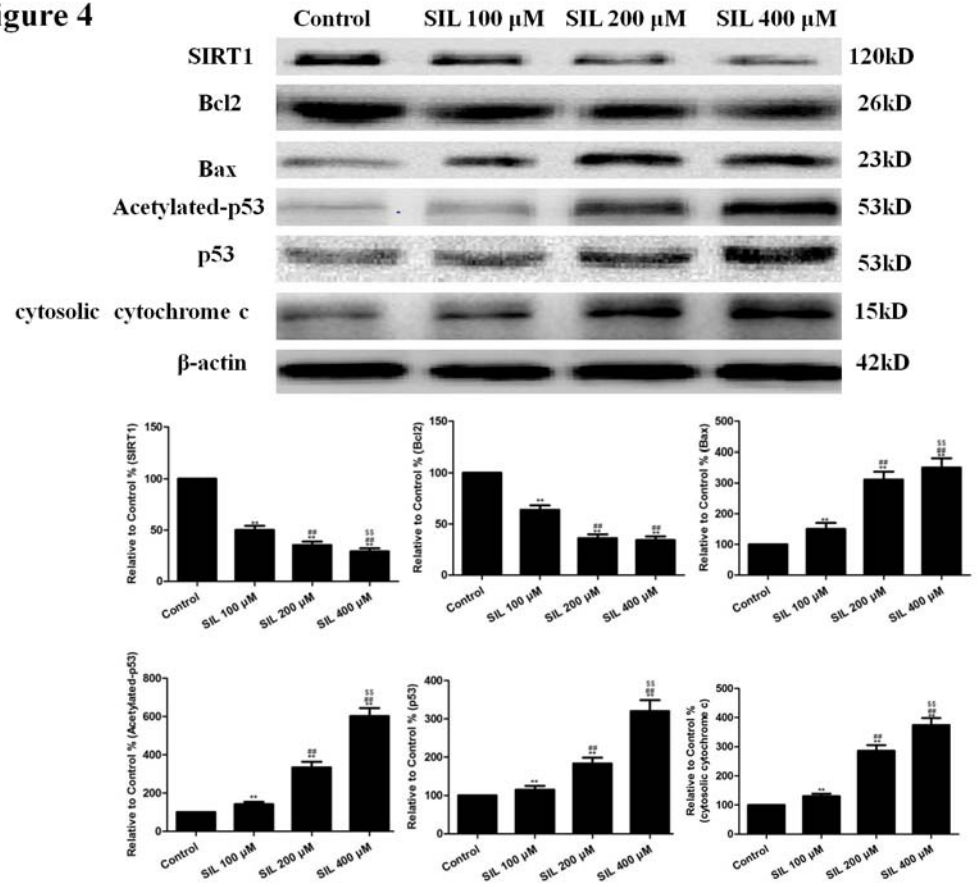

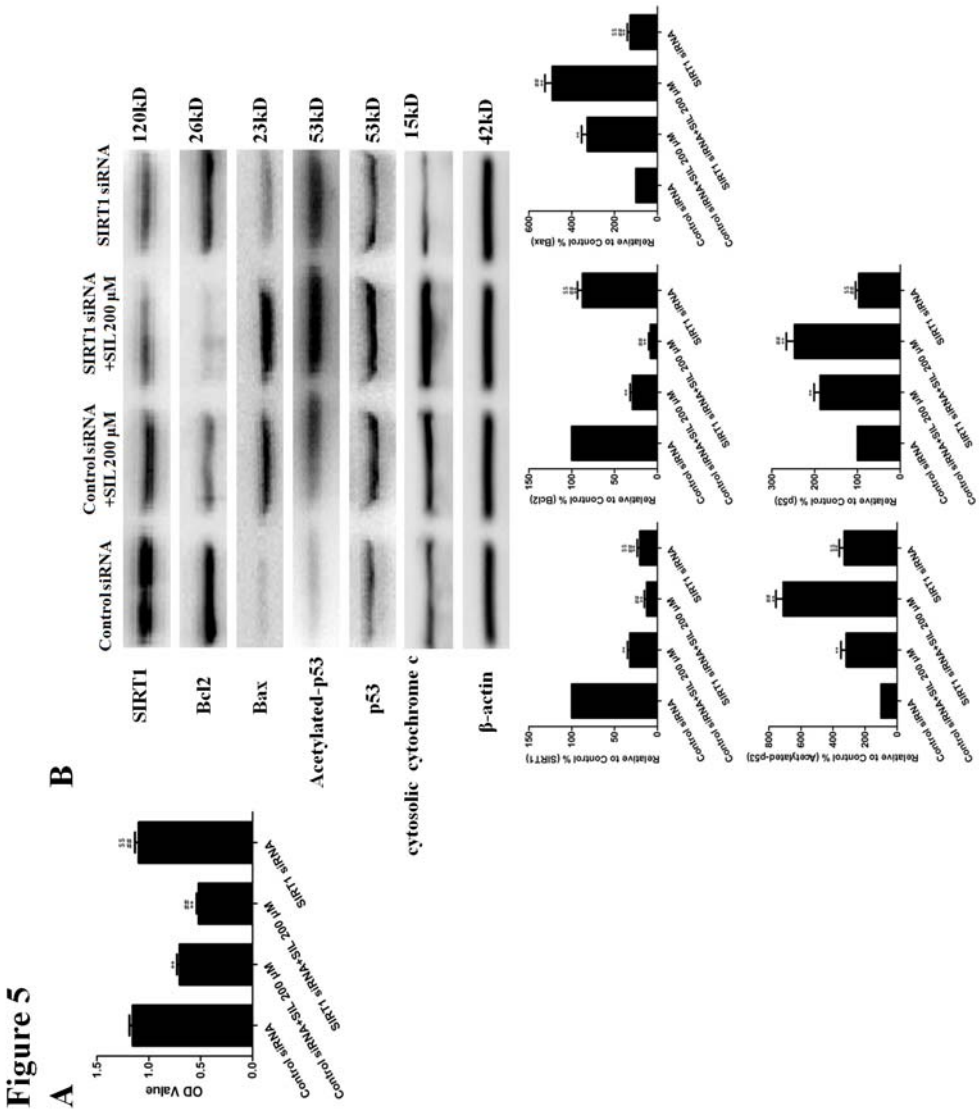

Figure 6

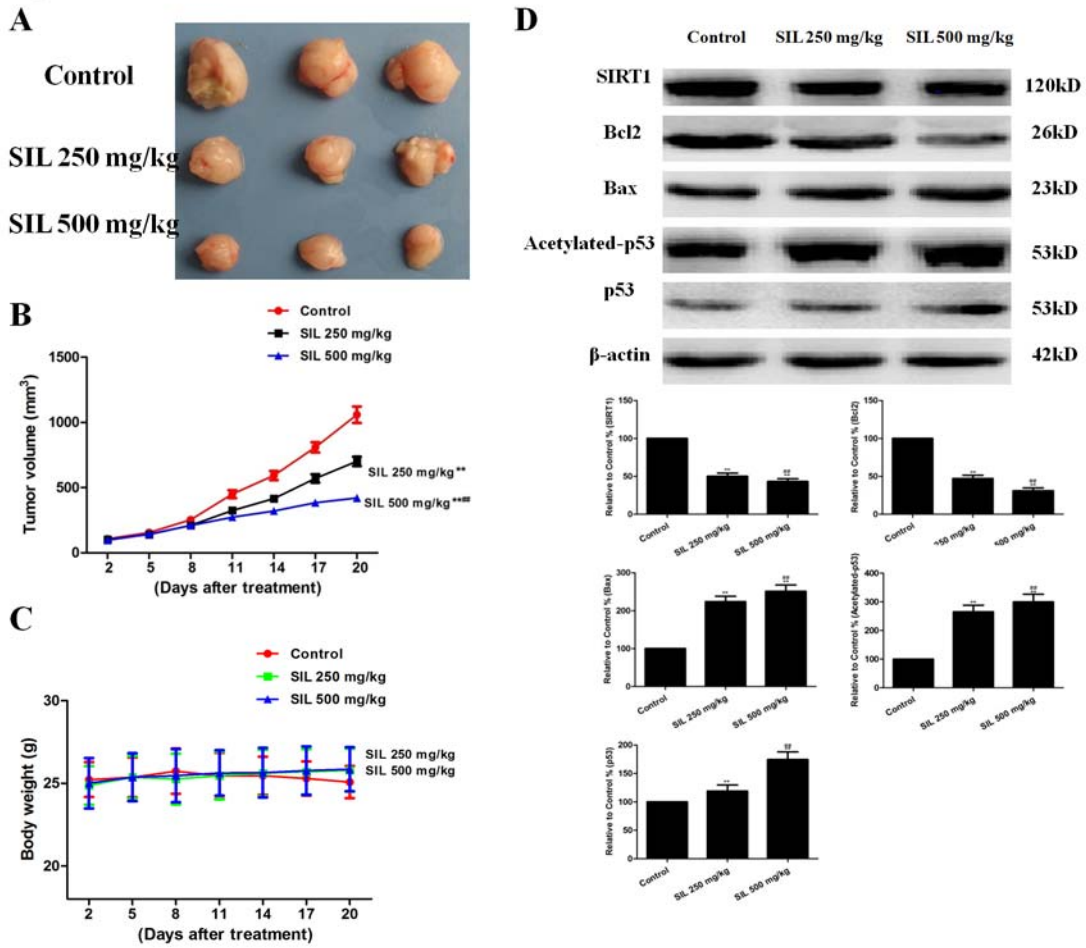

Figure 7

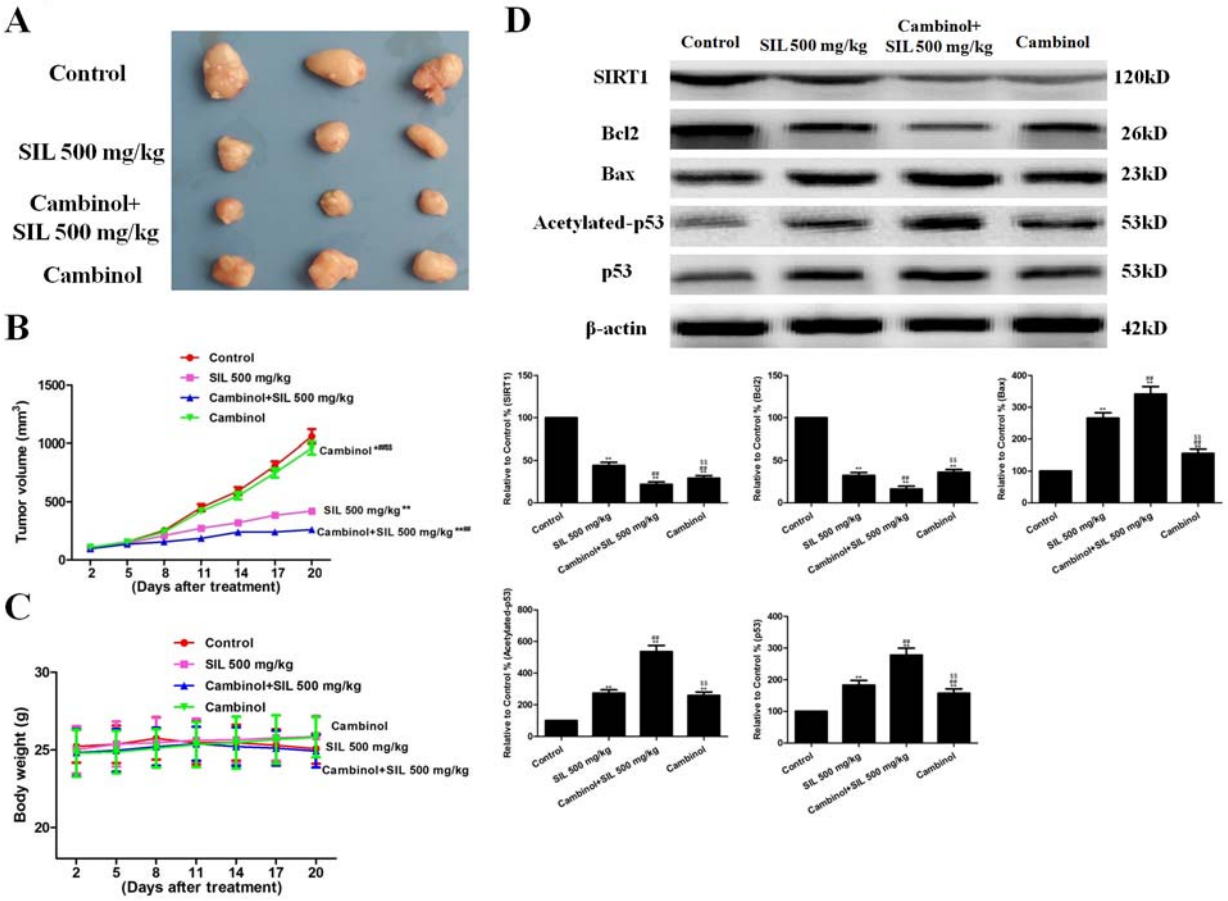

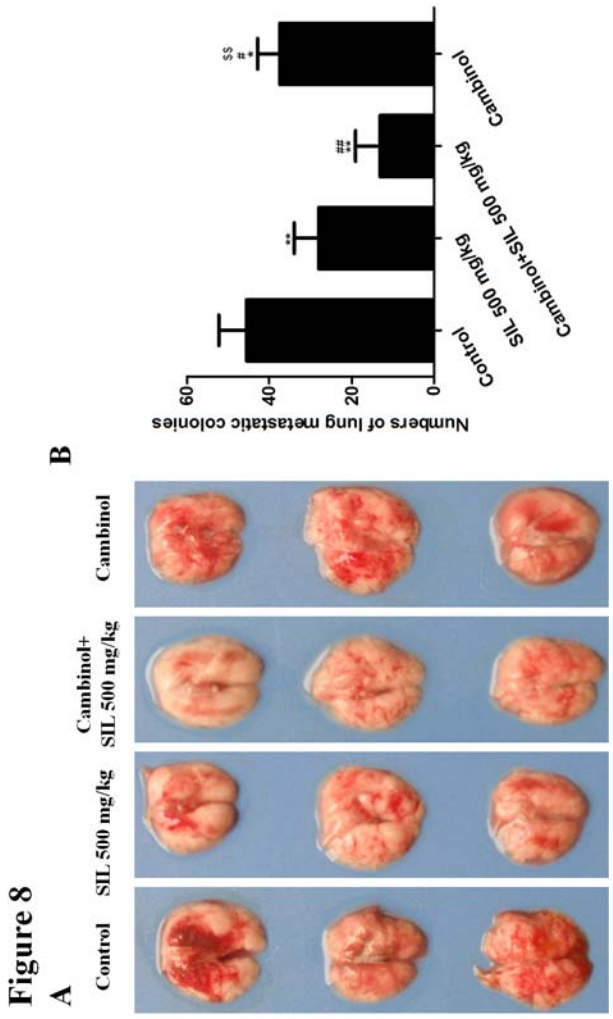

AACR American Association for Cancer Research

Molecular Cancer Therapeutics

Inhibition of SIRT1 signaling sensitizes the antitumor activity of silybin against human lung adenocarcinoma cells in vitro and in vivo

Zhenxing Liang, Yang Yang, Haibin Wang, et al.

Mol Cancer Ther Published OnlineFirst May 5, 2014.